Global NEST Journal, Vol 19, No X, pp XX-XX.

Synthesis and application of CeO_2/sawdust nanocomposite for removal of As(III) ions from aqueous solutions using a fixed bed column system

Hasanzadeh M.[1], Ansari R.[2*] and Ostovar F.[3]

[1]Department of Chemistry, Faculty of Science, University of Guilan, P.O.Box 41635-1914, Rasht, Iran
[2]Department of Chemistry, Faculty of Science, University of Guilan, P.O.Box 41635-1914, Rasht, Iran
[3]Department of Analytical Chemistry, Environmental research institute, Academic Center Culture & Research, Environmental Engineering, Rasht, Iran

Received: 21/03/2016, Accepted: 27/11/2016, Available online: 08/12/2016
*to whom all correspondence should be addressed:
e-mail: ransari271@guilan.ac.ir

Abstract: In this study, nanocomposite of ceria sawdust (CeO_2/SD) synthesized by precipitation method was utilized for removal of As (III) ions from aqueous solutions. Study of the process was done in column system. Characterization of the nano sized adsorbent particles was carried out using XRD and SEM techniques. The effects of important parameters, such as the value of initial pH, the flow rate, the influent concentration of arsenic and bed depth were studied in the column system. The Thomas model was applied for treatment of the adsorption data at different flow rate, influent concentration and bed depth. The bed-depth/service time analysis (BDST) model was also applied at different bed depth to predict the breakthrough curves. The two models were found suitable for describing the bio sorption process of the dynamic behavior of the CeO_2/SD adsorbent in column investigation. Based on Thomas model, the equilibrium adsorption reached 8.28 mg g^{-1} when a As(III) polluted solution with influent concentration of As 10 mg l^{-1} passed through the column with a flow rate of 2 ml min^{-1}. All the results suggested the presented nanocomposite as an efficient and cost effective adsorbent for removal of As (III) ions from aqueous solutions.

Keywords: Removal, As(III), CeO_2, Sawdust, Nanocomposite, Column system

1. Introduction

The main heavy metals which cause metal ion pollution are Cd, Pb, Cr, As, Hg, Cu and Ni and this metals generally refractory and cannot be degraded (AL-Othman *et al.,* 2012; Alqadami *et al.,* 2016; Naushad *et al.,* 2016). Arsenic (As) ranks 20th among the most abundant elements in the earth's crust, and it is associated with igneous and sedimentary rocks, particularly with sulphidic ores (Cullen and Reimer 1989; Abdullah *et al.,* 2016). Chemically, arsenic is very similar to its predecessor, phosphorus, and it can partially substitute for phosphorus in biochemical reactions. Arsenic is toxic to plants and soil biota (Sadiq 1997, Gaurav *et al.,* 2014). Long-term consumption of arsenic-contaminated water can lead to severe health problems, including skin lesions (e.g., pigmentation of the skin and the development of hard patches of skin on the palm of the hands), and kidney, lung, liver and prostate cancers (Rabiul Awual *et al.,* 2012). Arsenite, As (III), is generally considered to be more acutely toxic than arsenate, As(V) (Naqvi *et al.* 1994), and is also more potent than arsenate in chronic toxicity (Lantz *et al.,* 1994). The permissible limit (10 ppb) recommended by the World Health Organization (WHO, 2001) make no differentiation between arsenite and arsenate. Concentrations of arsenic detected in environment are generally reported as total arsenic (without regard to speciation) although some analytical methods are available to distinguish between the organic and inorganic forms and between the two valences states of arsenic (Butler, 1988; Guo *et al.,* 2007).

Arsenic is found in soils, air, and water as a metalloid and as chemical compounds of both inorganic and organic forms. Significant research has been completed in attempt to remove arsenic from aqueous solutions. Removal of As (V) and As (III) from groundwater has been researched using natural siderite in both batch and column studies (Guo *et al.,* 2007). Results for this research indicated that the high efficiency for As (III) rather than As (V) was attributed to adsorption of the As (III) to the pristine siderite and the fresh iron oxide coatings. In another study arsenic adsorption to Fe_2O_3 was shown to be higher than Al_2O_3 (Jeong *et al.,* 2007).

Using iron oxide for the removal of arsenite ions from groundwater showed that the removal was independent of both the arsenic and suspended solid concentrations. In

addition, ferrites have been shown to be more stable to dissolution than either metal hydroxides or metal sulfides (Zade and Dharmadhikari, 2007; Naushad *et al.,* 2015a). More recently nanomaterials have been studied for their ability to remove arsenic among other contaminants from aqueous solution, with much promise. For example, nanoscale zero valent iron is effective for the removal of arsenic through reduction mechanisms to elemental arsenic (Ramos *et al.,* 2009). Nanoparticles can also be surface modified for environmental applications. Iron nanoparticles have shown improved reactivity by coupling with catalytic metals (Obare and Meyer, 2004). Jeong found that adsorption to Fe_2O_3 was better than Al_2O_3, but neither of them had high adsorption capacities (Zade and Dharmadhikari, 2007; Naushad *et al.,* 2015b).

In the present study, nanoadsorbent CeO_2/SD was synthesized and studied for its ability to remove As(III) ions from aqueous solutions. The aim of this study is to develop a cheap technology for the removal of As (III) from wastewater. The nanocomposites were synthesized using a precipitation method, which consisted of a slow titration of soluble mixture with sodium hydroxide. The synthesized nanocomposite was then tested for the removal of As(III) from aqueous solution. Finally, studies were performed at the column system by CeO_2/SD nanocomposite. Several factors such as initial pH value, flow rate, influent concentration and bed depth on As(III) adsorption by CeO_2/SD column were considered. Thomas model and BDST model was used to predict the performance.

1.1. Thomas model

The data obtained in continuous mode studies was used to calculate maximum solid phase concentration of arsenic on adsorption rate constant using the kinetic model developed by Thomas (Thomas, 1944; Othman *et al.,* 2013). The Thomas model is one of the most general and widely used methods in column performance theory. The expression by Thomas for an adsorption column is given as follows:

$$\frac{C_t}{C_0} = \frac{1}{1+\exp\left[\frac{k_{TH}\left(q_0 x - C_0 V_{eff}\right)}{F}\right]} \quad (1)$$

where k_{Th} is the Thomas rate constant (ml min^{-1} mg^{-1}), q_0 the equilibrium arsenic uptake per g of the adsorbent (mg g^{-1}), x the amount of adsorbent in the column (g), V_{eff} the effluent volume (ml), C_0 the influent As(III) concentration (mg l^{-1}), C_t the effluent concentration at time t (mg l^{-1}) and F is the flow rate (ml min^{-1}). The value of C_t/C_0 is the ratio of effluent and influent arsenic concentrations. The value of time t (min) is $t = V_{eff}/F$. The kinetic coefficient K_{Th} and the adsorption capacity of the column q_0 can be determined from a plot of C_t/C_0 against t at a given flow rate.

1.2. The bed-depth/service time analysis (BDST) model

The BDST model is based on physically measuring the capacity of the bed at different breakthrough values. The BDST model works well and provides useful modeling equations for the changes of system parameters. A modified form of the equation that expresses the service time at breakthrough, t, as a fixed function of operation parameters is BDST model (Goel *et al.* 2005, Naushad *et al.* 2015c):

$$t = \frac{N_0}{C_0 F} Z - \frac{1}{K_a C_0} \ln\left(\frac{C_0}{C_t} - 1\right) \quad (2)$$

where C_t is the effluent concentration of solute in the liquid phase (mg l^{-1}), C_0 the initial concentration of solute in the liquid phase (mg l^{-1}), F the influent linear velocity (cm min^{-1}), N_0 the adsorption capacity (mg g^{-1}), K_a the rate constant in BDST model (l mg^{-1} min^{-1}), *t* the time (min) and *Z* is the bed depth of column (cm). A plot of *t* versus bed depth, *Z*, should yield a straight line where N_0 and *K*, the adsorption capacity and rate constant, respectively, can be evaluated.

2. Materials and methods

2.1. Materials

All chemicals used were of analytical grade (AR) and were prepared in distilled water. The sulfate or chloride salts of all cations were purchased from Merck with highest purity available and used without any further purification. All experiments were carried out in aqueous solutions using distilled water. A Metrohm pH meter (model 827) with a combined double junction glass electrode, calibrated against two standard buffer solutions at pH 4.0 and 7.0, was used for pH measurement. The pH of the solutions was adjusted using either 0.10 M HCl or NaOH solutions.

2.2. Preparation of CeO_2/SD

For preparation of, 4.5 g sawdust was added to 90 mL of 0.10 M $Ce(SO_4)_2$ solution and stirred for two hours at room temperature. Afterwards, NaOH solution (0.4 M) was slowly added into the mixture of metal ion-sawdust under vigorous steering and then mixture was heated at 80 °C for another 2h. Subsequently, CeO_2/SD particles were rinsed with sufficient deionized water and dried for several hours in an oven at 100 °C.

2.3. Preparation of As(III) test solutions

As_2O_3 was used as the source of As (III). Stock solutions of 100 mg l^{-1} of As(III) ions were prepared by dissolving As_2O_3 in NaOH solution, and then the pH was adjusted to 5 using 0.10 M HCl. All working solutions were prepared by diluting the stock solution with distilled water to the needed concentration.

2.4. Adsorption experiments

Continuous flow sorption experiments were conducted in a glass column (1 cm internal diameter and 50 cm height). CeO_2/SD nanocomposite was packed into a glass column (1 cm in diameter and 60 cm in height). Except the experiment of the effect of pH values and bed depth, the mass of CeO_2/SD in the column was 0.50 g and the value of pH was about 5 (the natural value). In considering of pH effect, the pH of arsenic solutions was adjusted by adding either 0.1 M HCl or NaOH solution. Samples were collected at regular

time intervals in all the adsorption. Determination of ascorbic acid was carried out by iodometric coulometric titration. Platinum and silver wires were used as working (anode) and counter (cathode) electrodes in, respectively. Excess of potassium iodide was used as auxiliary electrolyte and starch was used as indicator helping to detect the endpoint. A Digital coulometer (ZAG Chemie Co.) was used for recording of the charge consumed during titration. In order to study the effect of bed depth for determination of the column performance, the experiments were conducted at different bed depth, 1.5 cm (0.25 g), 3 cm (0.5 g), 4.5 cm (0.75 g) with influent As(III) concentration of 10 mg l^{-1} and flow rate of 2 ml min^{-1}.

2.5. Characterizations

The synthesized CeO_2/SD nanocomposite were characterized by the techniques usually employed in porous materials, such as power X-ray diffraction (XRD) using an Philips PW X-ray diffractometer at a voltage of 40 kV and a current of 100 mA with Cu K∝ radiation (ƛ=1.54056 A˚), in the 2θ ranging from 0 to 70. The surface morphology and particle size of the products were measured using Scanning electron microscopy with unique thermo-emission electron source by a tungsten film, Germany and UK Co-production model LEO 1430VP). The infrared spectra (400–4000 cm^{-1}) of samples were recorded on an alpha FT-IR (2011 Bruker Optic GmbH) instrument.

3. Results and discussion

3.1. Characterization of CeO_2/Sawdust nanocomposite

3.1.1. XRD Studies

Fig. 1 shows the XRD pattern of CeO_2 NPs, untreated Sawdust and CeO_2/SD nanocomposite prepared via chemical precipitation method.

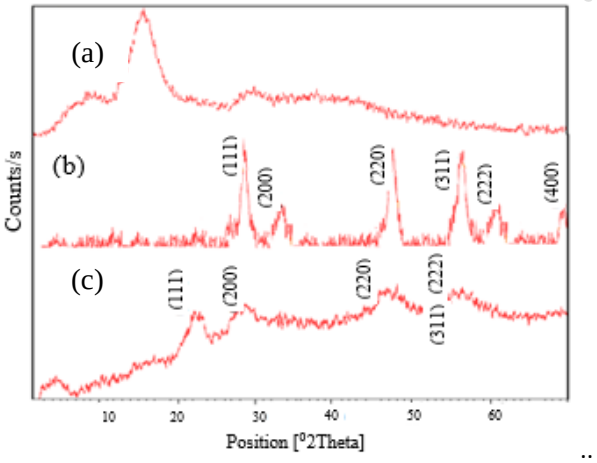

Figure 1. XRD patterns of synthesized (a) CeO_2/SD, (b) CeO_2 NPs and (c) untreated Sawdust

The XRD pattern of sawdust is presented in Figure 1a. In Figure 1a, the bulk of the X-ray signal originated from the sawdust substrate. The XRD peaks of pure CeO_2 (Fig 1 b) at 2θ of 28.60°, 33.20°, 47.40°, 56.40°, 59.10° and 69.40° were respectively indexed as (111), (200), (220), (311), (222) and (400) phases, corresponding to a face-centered cubic (FCC) fluorite structure for CeO_2 (Zhou and Switzer, 1996). As shown, Index peaks of CeO_2 are clearly observed in the synthesized CeO_2/SD nanocomposite (Fig 1c). The intensity of reflections in CeO_2/SD NC was decreased via a layer of Cerium oxide nanoparticles covered on the sawdust due to interactions with sawdust.

3.1.2. Surface Morphological studies

Scanning electron microscope (SEM) pictures are useful for examining the fine structure of materials. SEM technique is commonly used for surface characterization and determination of particle size, shape as well as particle size distribution in nanomaterials. The SEM micrographs of the synthesized CeO_2/SD before and after As(III) solution treatment are shown in Figs. 2. The non-uniform and segregate CeO_2 nano-sized particles coated onto sawdust are presented in Fig. 2a. As indicated, the particle sizes are affected when the CeO_2/SD nanocomposite treated with the arsenic solution (Fig. 2b).

3.1.3. FT-IR spectroscopy study

The FTIR spectra of the untreated sawdust, CeO_2 NPs, CeO_2/SD NC before and after adsorption are shown in Figure 3 and 4. The FTIR measurements were done by using the KBr pellet technique (Mazaheri *et al.,* 2009). Figure 3a shows the FT-IR spectra of untreated sawdust. Sawdust has a fiber structure and its main component is cellulose, which has a straight chain structure and large molecule mass. The adsorption peak at 3411 cm^{-1} indicates the hydroxyl groups and the adsorption band at 2905 cm^{-1} is due to the contribution from C-H stretching. The band at 2359 cm^{-1} is assigned to stretching vibrations of N–H or C=O groups probably due to amines and ketones, 1647 cm^{-1} is an indication of COO, C=O, and can also indicate the bending vibration of adsorbed water, 1268 cm^{-1} is assigned to carboxylic acids vibration, 1058 cm^{-1} is stretching vibration of C–O–C and O–H of polysaccharides. The band at around 1428 cm^{-1} is assigned to symmetric COO– stretching motions and to the bending vibrations of aliphatic groups, whereas the peak at 1372 cm^{-1} refers to C-O stretching of cellulose in sawdust (Moafi *et al.,* 2016). The infrared spectrum (FTIR) of CeO_2 nanoparticles was in the range of 400-4000 cm^{-1} wave number and identifies the chemical bonds, as well as functional groups in the compound shows in Figure 3b. The absorption peak at 3436 cm^{-1} indicates the stretching vibration hydroxyl groups. Several broad absorption peaks centered at 1636 cm^{-1}, 1333 cm^{-1}, 1188 cm^{-1} and 1106 cm^{-1} indicate the existence of functional groups that are a bending vibration of C-H stretching. The strong band below 700 cm^{-1} was assigned to the Ce-O stretching mode (Reinhardt *et al.,* 2002). The broad band, corresponding to the Ce-O stretching banding of CeO_2 is seen at 506 cm^{-1}. Figure 3c shows the FT-IR spectra of CeO_2/SD NC. The vibration and stretching peaks such as OH^- groups, C-H stretching and stretching of cellulose of sawdust was shown. The peaks located in the area from 400 to 750 cm^{-1} to the CeO_2 stretching. The rest of the peaks were also similar with each other which indicate the formation of pure phase of CeO_2. FT-IR spectra of CeO_2/SD NC after adsorption of As (III) is shown in Figure 4. The

adsorption peaks for main component of sawdust and functional groups in the CeO_2 nanoparticles into the CeO_2/SD nanocomposite such as fiber structure, cellulose and stretching vibration hydroxyl groups, vibration of C-H stretching, Ce-O stretching mode, respectively are shifted to 3432.36 cm^{-1}, 2356.58 cm^{-1}, 1635.88 cm^{-1}, 540.69 cm^{-1} after adsorption indicates the adsorption of arsenic (III) ions.

3.2. Column Adsorption Study

3.2.1. The effect of pH

To investigate the effect of pH on the As(III) adsorption, As(III) solution (C=10 mg L^{-1}) was passed through the column containing CeO_2/SD particles at various pH values (3, 5 and 10). Fig 5 shows the effect of pH value on adsorption of As(III) onto CeO_2/SD using a plot of dimensionless concentration (C_t/C_0) versus volume of influent solution (mL). As indicated the adsorption capacity of the column is highly dependent on the pH of the solution. The maximum adsorption occurred at pH value about 5 to 6.

3.2.2. The effect of flow rate

To investigate the effect of flow rate on arsenic adsorption, the influent arsenic concentration was held constant at 10 mg L^{-1}, and test solution passed through the column at three different flow rates (2.0, 5.0 and 8.0 ml min^{-1}). The breakthrough curves obtained are shown in Fig 6. The variation in the slope of the breakthrough curve and adsorption capacity may be explained on the basis of mass transfer fundamentals. As represented, the breakpoint occurred faster at higher flow rate. The reason is that at higher flow rate the rate of mass transfer gets increases, i.e. the amount of cation adsorbed onto unit bed height (mass transfer zone) gets increased with increasing flow rate leading to faster saturation at higher flow rate (Ko *et al.,* 2000). In contrast, breakthrough time reaching saturation was increased significantly with a decreased in the flow rate. Since at a low influent flow rate, the adsorbate has more time to contact with CeO_2/SD that resulted in higher removal.

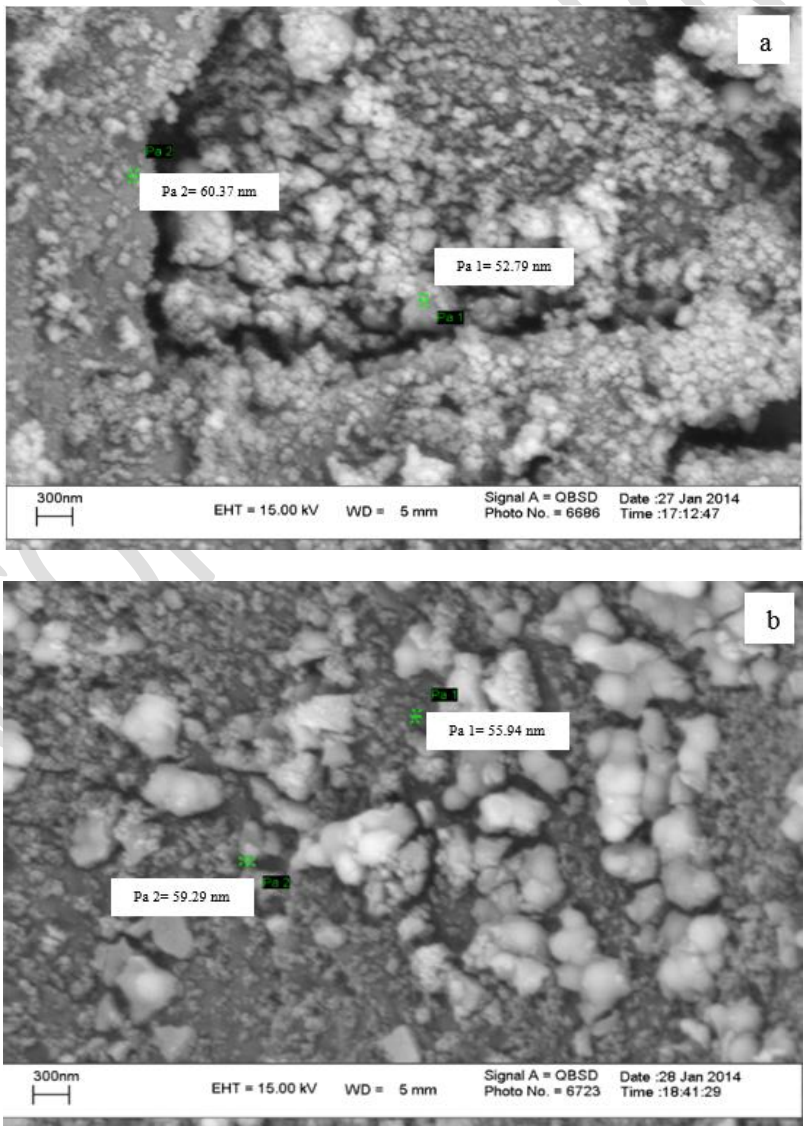

Figure 2. Scanning electron microscopy (SEM) images of CeO_2/SD, (a) before & (b) after As (III) adsorption

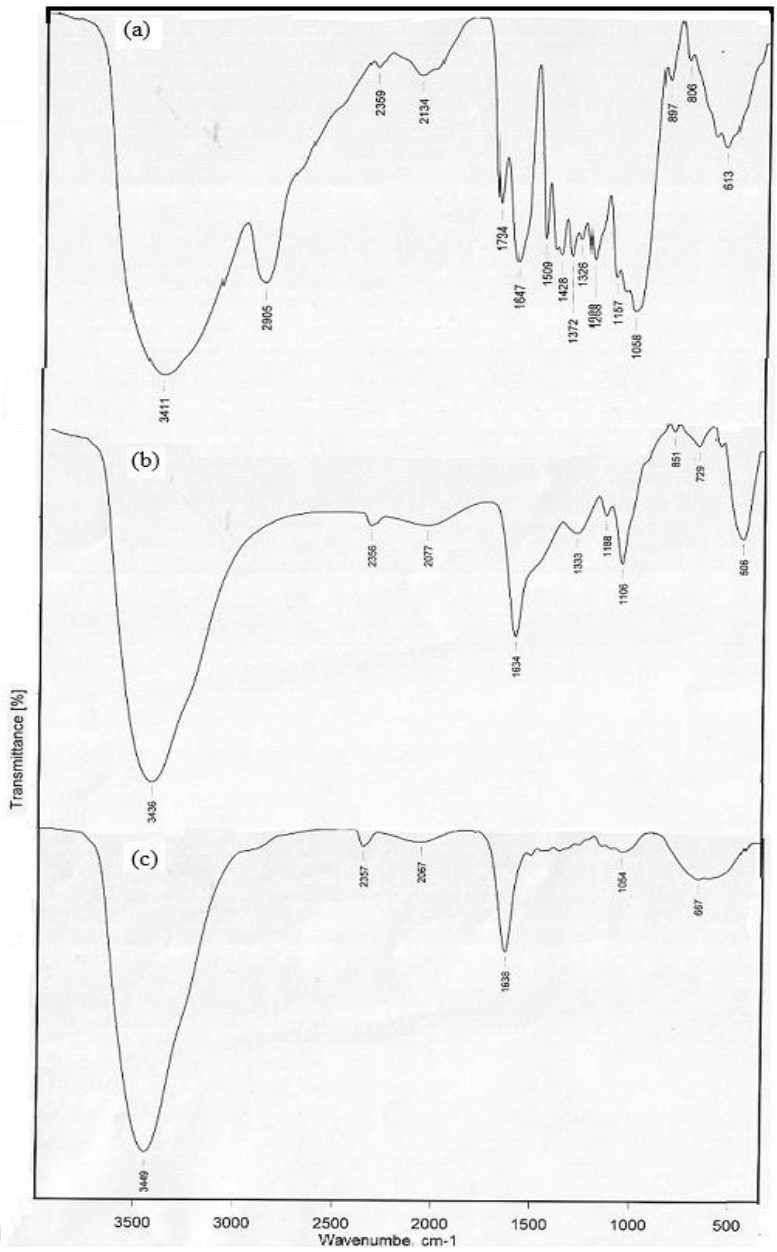

Figure 3. FT-IR spectra of a) untreater Sawdast, b) CeO_2 NPs and c) CeO_2/SD NC before As(III) adsorption

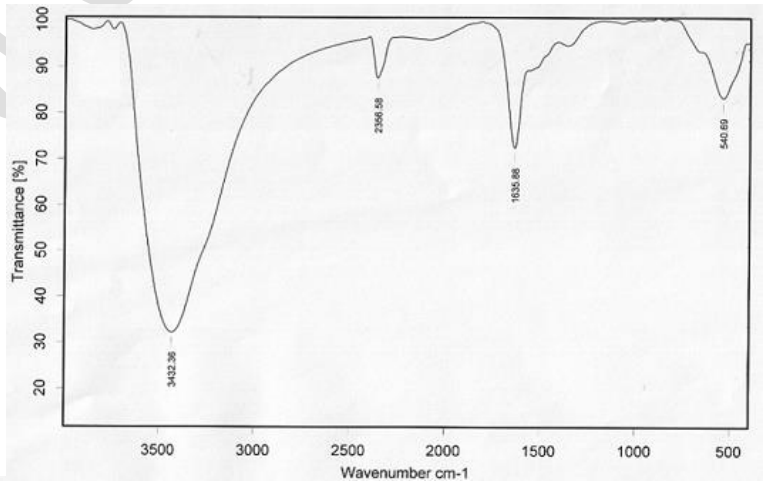

Figure 4. FT-IR spectra of a) CeO_2/SD NC after As(III) adsorption

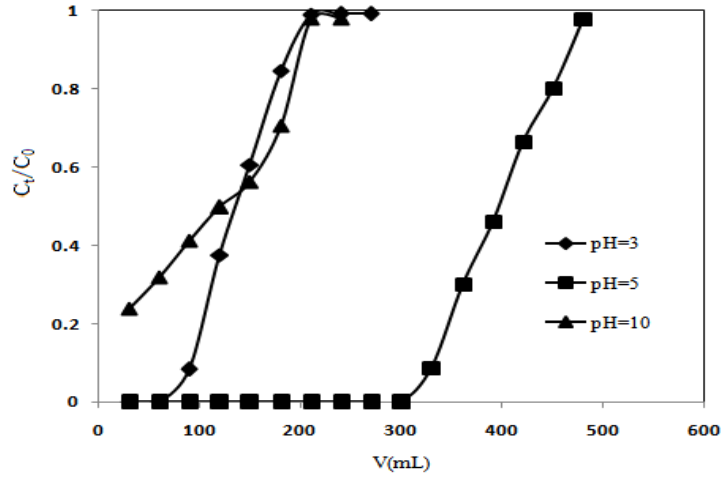

Figure 5. Breakthrough curves of the effect of pH values (F.r = 2 mL min^{-1}, C_0 =10 mg l^{-1})

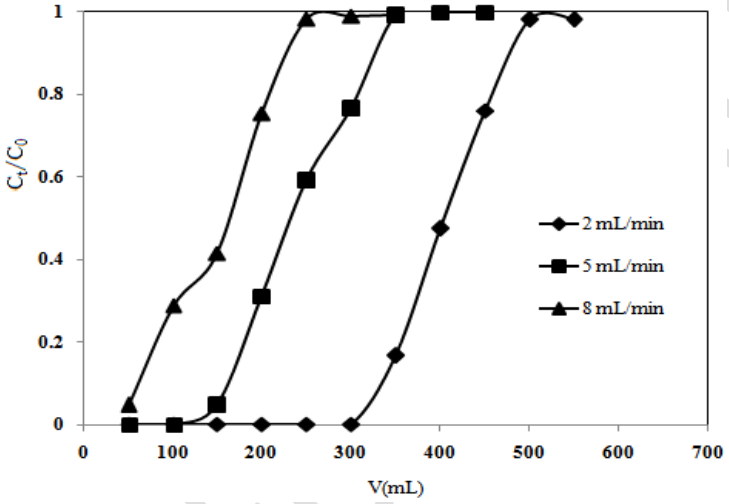

Figure 6. Breakthrough curves of the effect of flow rate (C_0 =10 mg l^{-1})

3.2.3. Effect of influent Arsenic concentration

The effect of influent arsenic concentration on the shape of the breakthrough curves was shown in Fig 7. It is illustrated that the breakthrough time decreased with increasing influent arsenic concentration. As influent concentration increased, sharper breakthrough curves were obtained. These results demonstrate that the change of concentration gradient affects the saturation rate and breakthrough time. As the influent concentration increases, cation loading rate increases, so does the driving force increase for mass transfer, which in a decrease in the adsorption zone length (Goel *et al.* 2005).

3.2.4. The effect of bed depth

Fig 8 was the breakthrough curve at different bed depth at the same influent concentration (C_0 =10 mg l^{-1}) and flow rate (F.r =2 ml min^{-1}), respectively. From Fig 6, as the bed height increases, As (III) polluted solution had more time to contact with CeO_2/SD that resulted in higher removal efficiency of arsenic ions in column. The slope of breakthrough curve decreased with increasing bed height, which resulted in a broadened mass transfer zone. High uptake was observed at the highest bed height due to an increase in the surface area of bio-sorbent, which provided more binding sites for the sorption (Vijayaraghavan *et al.,* 2004). 3.3. Modeling of column study results

3.3.1. BDST model

The BDST model is based on physically measuring the capacity of the bed at different breakthrough values. This simplified design model ignores the intra particle mass transfer resistance and external film resistance such that the adsorbate is adsorbed onto the adsorbent surface directly.

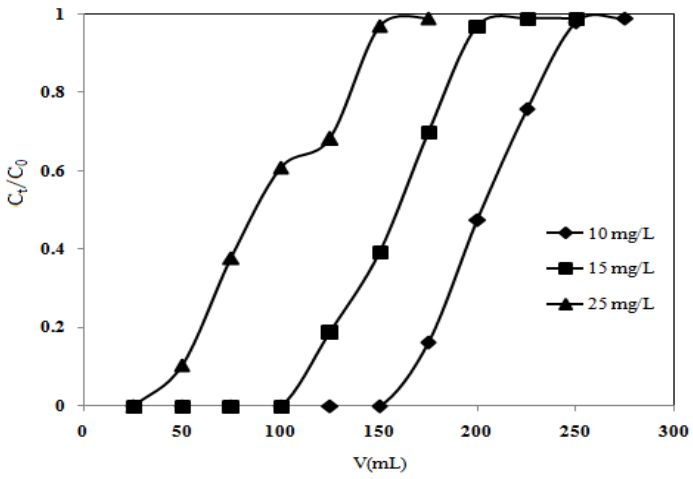

Figure 7. Breakthrough curves of the effect of influent concentration (F.r=2 mL min^{-1})

With these assumptions, the BDST model works well and provides useful modeling equations for the changes of the system parameters (Ko *et al.,* 2000). The line of t–z at value of C_t/C_0 = 0.6 is shown in Fig. 9.

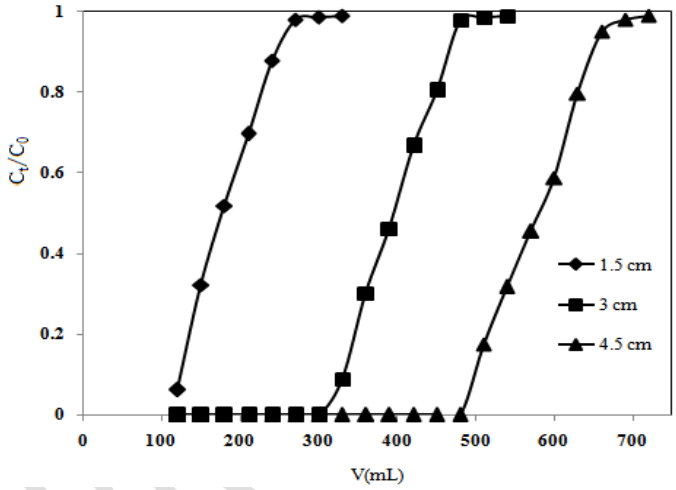

Figure 8. Breakthrough curves of the effect of bed depth (F.r = 2 mL min^{-1}, C_0 =10 mg L^{-1})

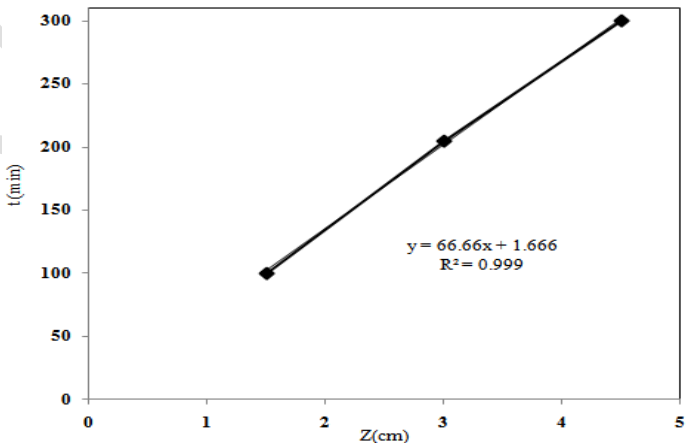

Figure 9. The linear plot of t versus z for 0.6 obtained from the resulted breakthroughs at different bed heights (F.r = 2 mL min^{-1}, C_0 =10 mg L^{-1})

The BDST model parameters can be helpful to scale up the process for other flow rates without further experimental run. The related constants of BDST according to the slopes and intercepts of the lines are listed in Table 1. The adsorption capacity of the bed per unit bed volume, N_0, was calculated from the slope of BDST plot, assuming initial

concentration, C_0, and linear velocity, F, is constant during the column operation.

3.3.2. Thomas model

Thomas model was applied to the experimental data with respect to flow rate, influent concentration of As (III) and bed depth. A non-linear regression analysis was used on each set of data to determine the Thomas model parameters of q_0 and K_{Th}. The results were listed in Table 2. They were all fits with higher determined coefficients (R^2) ranging from 0.995 to 0.999. As shown in Table 2, as the influent concentration increased, the value of q_0 increased but the value of K_{Th} decreased. The reason is that the driving force for bio-sorption is the concentration difference between the Pollutant on the bio-sorbent and the Pollutant in the solution (Aksu and Onen, 2003). Thus the high driving force due to the higher As (III) concentration resulted in better column performance.

Table 1. Calculated parameters of BDST model (C_0 =10 mg L^{-1})

C_t/C_0	F (mL.min^{-1})	w(g)	N_0(mg.g^{-1})	K_a(L.mg^{-1}.min^{-1})	R^2
0.2	2	0.5	1444.89	0.039	0.995
0.4	2	0.5	1614.91	-0.0121	0.999
0.6	2	0.5	1699.83	-0.024	0.999

As shown with flow rate increasing, the value of q_0 decreased but the value of K_{Th} increased. As the bed depth increased, the value of q_0 increased significantly while the value of K_{Th} decreased significantly. So higher flow rate and lower influent concentration have disadvantage to adsorption of As (III) on CeO_2/SD column.

Table 2 Calculated parameters of Thomas model at different conditions

C_0	F (mL.min^{-1})	w(g)	K_{th}	$q_{0,cal.}$	$q_{0,exp.}$	R^2
10	2	0.5	0.0047	8.28	7.46	0.914
15	2	0.5	0.0045	7.99	7.59	0.981
25	2	0.5	0.0044	7.81	7.71	0.997

Comparison of the maximum adsorption capacities of more adsorbents for arsenic adsorption are listed in Table 3.

3.4. Arsenic adsorption/desorption mechanism

Once the sorbent becomes exhausted, the As(III) ions must be recovered and the sorbent regenerated. Desorption and sorbent regeneration is very important. The primary objective of regeneration is to restore the adsorption capacity of the exhausted adsorbent while the secondary objective is to recover valuable components present in the adsorbed phase. In this study, various chemicals such as NaOH, HCl, NaCl etc. were tested to recover the adsorbed As(III) ions from the saturated adsorbent (CeO_2/SD NC).

Table 3. Maximum adsorption capacity of various commercial adsorbents for removal of As(III) from aqueous samples

Adsorbents	Adsorption Capacity (mg g^{-1})	Reference
ZVI nanoparticles	3.5	(Daikopoulos *et al.*, 2014)
Iron modified jute fibres	12.66	(Hao *et al,* 2015)
Iron oxide coated cement (~0.212 mm)	0.69	(Sanghamitra *et al.,* 2007)
Fe_2O_3 nanomaterial	1.25	(Ye *et al*., 2011)
Iron oxide-coated sand	0.029	(Thirunavukkarasu *et al*., 2003)
Waste rice husk	0.02	(Amin *et al.,* 2006)
Activated alumina (AA)	0.384	(Singh *et al.,* 2006)
CeO_2/SD NC	7.46	Present study

Solution of As(III) with concentration of 10 mg l was passed through the column with flow rate of 2 ml min^{-1}. The results showed that an unsuccessful desorption process must restore the sorbent close to its initial properties for effective reuse. So, the synthesis adsorbent can't be used as As(III) adsorbent for several consecutive times.

4. Conclusions

On the base of the experimental results of this investigation, the following conclusion can be drawn: The introduced nanocomposite in the current work (CeO_2/SD) was found to be a highly efficient adsorbent for As (III) removal from aqueous solutions in non-equilibrium or column system. Variables, such as pH, influent concentration, bed depth and flow rate can affect the breakthrough curve. The Thomas model and BDST model adequately described the adsorption of As (III) onto CeO_2/SD by column mode. Due to the high toxicity of As (III) ions, the findings in the current research seem to be very important from environmental point of view and arsenic removal technology.

Acknowledgement

The authors appreciate the Research Department of University of Guilan for partially financial support of this work.

References

Alqadami A.A., Naushad M., Abdalla M.A., Ahamad T., Alothman Z.A. and Alshehri S.M. (2016), Synthesis and characterization of Fe_3O_4@ TSC nanocomposite: highly efficient removal of toxic metal ions from aqueous medium, *RSC Advances*, **6**(27), 22679-22689.

Alqadami A.A., Naushad M., Abdalla M.A., Khan M.R., and Alothman Z.A. (2016), Adsorptive Removal of Toxic Dye Using Fe_3O_4–TSC Nanocomposite: Equilibrium, Kinetic, and Thermodynamic Studies, *Journal of Chemical and Engineering Data*, **61**(11), 3806–3813.

Aksu Z. and Gönen F. (2004), Biosorption of phenol by immobilized activated sludge in a continuous packed bed: prediction of breakthrough curves, *Process biochemistry*, **39**(5), 599-613.

Al-Othman Z.A., Ali R. and Naushad M. (2012), Hexavalent chromium removal from aqueous medium by activated carbon prepared from peanut shell: adsorption kinetics, equilibrium and thermodynamic studies, *Chemical Engineering Journal*, **184**, 238-247.

Amin M.N., Kaneco S., Kitagawa T., Begum A., Katsumata H., Suzuki T. and Ohta K. (2006), Removal of arsenic in aqueous solutions by adsorption onto waste rice husk, *Industrial and engineering chemistry research*, **45**(24), 8105-8110.

Awual M.R., Shenashen M.A., Yaita T., Shiwaku H. and Jyo A. (2012), Efficient arsenic (V) removal from water by ligand exchange fibrous adsorbent, *water research*, **46**(17), 5541-5550.

Butler E.C.V. (1988), Determination of inorganic arsenic species in aqueous samples by ion-exclusion chromatography with electro-chemical detection, *Journal of Chromatography A*, **450**(3), 353-360.

Cullen W.R. and Reimer K.J. (1989), arsenic speciation in the environment, *Chemical Reviews*, **89**(4), 713-764.

Daikopoulos C., Georgiou Y., Bourlinos A.B., Baikousi M., Karakassides M.A., Zboril R., Steriotis T.A. and Deligiannakis Y. (2014), Arsenite remediation by an amine-rich graphitic carbon nitride synthesized by a novel low-temperature method, *Chemical* Engineering *Journal*, **256**, 347-355.

Geneva (2001), Arsenic in Drinking Water, *World Health Organization*, Switzerland, Fact Sheet, 210.

Goel J., Kadirvelu K., Rajagopal C. and Garg V.K. (2005), Removal of lead (II) by adsorption using treated granular activated carbon: batch and column studies, *Journal of Hazardous Materials*, **125**(1), 211-220.

Guo H., Stüben D. and Berner Z. (2007), Adsorption of arsenic (III) and arsenic (V) from groundwater using natural siderite as the adsorbent, *Journal of Colloid and Interface Science*, **315**(1), 47-53.

Hao L., Zheng T., Jiang J., Hu Q., Li X. and Wang P. (2015), Removal of As (III) from water using modified jute fibres as a hybrid adsorbent, *RSC Advances*, **5**(14), 10723-10732.

Jeong Y., Fan M., Singh S., Chuang C.L., Saha B. and Van Leeuwen J.H. (2007), Evaluation of iron oxide and aluminum oxide as potential arsenic (V) adsorbents, *Chemical Engineering and Processing: Process Intensification*, **46**(10), 1030-1039.

Ko D.C., Porter J.F. and McKay G. (2000), Optimised correlations for the fixed-bed adsorption of metal ions on bone char, *Chemical engineering science*, **55**(23), 5819-5829.

Kundu S. and Gupta A.K. (2007), Adsorption characteristics of As (III) from aqueous solution on iron oxide coated cement (IOCC), *Journal of Hazardous Materials*, **142**(1), 97-104.

Lantz R.C., Parliman G., Chen G.J. and Carter D.E. (1994), Effect of arsenic exposure on alveolar macrophage function: I. Effect of soluble As (III) and As (V), *Environmental research*, **67**(2), 183-195.

Mazaheri M., Hassanzadeh-Tabrizi S.A., Aminzare M. and Sadrnezhaad S.K. (2010), Synthesis of CeO_2 nanocrystalline powder by precipitation method, *Materiały Ceramiczne*, **62**(4), 529-532.

Fallah Moafi H., Ansari R. and Ostovar F. (2016), Ag_2O/Sawdust nanocomposite as an efficient adsorbent for removal of hexavalent chromium ions from aqueous solutions, *Journal of Materials and Environmental Science,* **7**(6) 2051-2068.

Naqvi S.M., Vaishnavi C. and Singh H. (1994), Toxicity and metabolism of arsenic in vertebrates, *Advances in Environmental Science and Technology -New York*, **27**, 55-55.

Naushad M. and ALOthman Z.A. (2015), Separation of toxic Pb^{2+} metal from aqueous solution using strongly acidic cation-exchange resin: analytical applications for the removal of metal ions from pharmaceutical formulation, *Desalination and Water Treatment*, **53**(8), 2158-2166.

Naushad M., Ahamad T., Sharma G., Ala'a H. Albadarin A. B., Alam M.M., ALOthman Z. A., Alshehri S.M. and Ghfar A.A. (2016), Synthesis and characterization of a new starch/SnO_2 nanocomposite for efficient adsorption of toxic Hg^{2+} metal ion, *Chemical Engineering Journal*, **300**, 306-316.

Naushad M., ALOthman Z.A. and Sharma G. (2015), Kinetics, isotherm and thermodynamic investigations for the adsorption of Co (II) ion onto crystal violet modified amberlite IR-120 resin, *Ionics*, **21**(5), 1453-1459.

Naushad M., ALOthman Z.A. and Javadian H. (2015), Removal of Pb (II) from aqueous solution using ethylene diamine tetra acetic acid-Zr (IV) iodate composite cation exchanger: Kinetics, isotherms and thermodynamic studies, *Journal of Industrial and Engineering Chemistry*, **25**, 35-41.

Obare S.O. and Meyer G.J. (2004), Nanostructured materials for environmental remediation of organic contaminants in water, *Journal of Environmental Science and Health, Part A*, **39**(10), 2549-2582.

ALOthman Z.A., Naushad M. and Ali R. (2013), Kinetic, equilibrium isotherm and thermodynamic studies of Cr (VI) adsorption onto low-cost adsorbent developed from peanut shell activated with phosphoric acid, *Environmental Science and Pollution Research*, **20**(5), 3351-3365.

Ramos M.A., Yan W., Li X.Q., Koel B.E. and Zhang W.X. (2009), Simultaneous oxidation and reduction of arsenic by zero-valent iron nanoparticles: Understanding the significance of the core− shell structure, *The Journal of Physical Chemistry C*, **113**(33), 14591-14594.

Reinhardt K. and Winkler H. (2002), Cerium mischmetal, cerium alloys, and cerium compounds, in: Ullmann's encyclopedia of industrial chemistry, *Weinheim, Germany: Wiley-VCH*, **7**, 285–300.

Sadiq M. (1997), Arsenic chemistry in soils: an overview of thermodynamic predictions and field observations, *Water, air and soil pollution*, **93**(1-4), 117-136.

Sharma G., Pathania D., Naushad M. and Kothiyal N.C. (2014), Fabrication, characterization and antimicrobial activity of polyaniline Th(IV) tungstomolybdophosphate nanocomposite

material: Efficient removal of toxic metal ions from water, *Chemical Engineering Journal*, **251**, 413-421.

Singh T.S. and Pant K.K. (2006), Experimental and modelling studies on fixed bed adsorption of As (III) ions from aqueous solution, *Separation and Purification Technology*, **48**(3), 288-296.

Thirunavukkarasu O.S., Viraraghavan T. and Subramanian K.S. (2003), Arsenic removal from drinking water using iron oxide-coated sand, *Water, air and soil pollution*, **142**(1-4), 95-111.

Thomas H.C. (1944), Heterogeneous ion exchange in a flowing system, *Journal of the American Chemical Society*, **66**(10), 1664-1666.

Tian Y., Wu M., Lin X., Huang P. and Huang Y. (2011), Synthesis of magnetic wheat straw for arsenic adsorption, *Journal of hazardous materials*, **193**, 10-16.

Vijayaraghavan K., Jegan J., Palanivelu K. and Velan M. (2004), Removal of nickel (II) ions from aqueous solution using crab shell particles in a packed bed up-flow column, *Journal of hazardous materials*, **113**(1), 223-230.

Zade P. D. and Dharmadhikari D.M. (2007), Removal of arsenic as arsenite from groundwater/wastewater as stable metal ferrite, *Journal of Environmental Science and Health Part A*, **42**(8), 1073-1079.

Zhou Y. and Switzer J.A (1996), Growth of cerium (IV) oxide films by the electrochemical generation of base method, *J alloys compounds*, **237**(1), 1-5.